1

Neutron Radiography Evaluation of Drying in Mortars with and without Shrinkage Reducing Admixtures

C. Villani[1], C. Lucero[1], D. Bentz[2], D. Hussey[2], D.L. Jacobson[2] and W. J. Weiss[1]

1. Lyles School of Civil Engineering, Purdue University, West Lafayette, IN
2. National Institute of Standards and Technology

Biography:

Chiara Villani is a Post-Doctoral Research Assistant at Purdue University. She received her PhD from Purdue University and her BS and MS in Civil Engineering from the Polytechnic of Turin. Her research interests include drying processes in cementitious materials, durability of concrete structures and characterization of sustainable cementitious composites.

Catherine Lucero is a master's research assistant at Purdue University. She received her BS in civil engineering from the University of New Mexico in Albuquerque. Her research focuses on using neutron imaging to assess fluid transport in concrete.

ACI member Dale P. Bentz is a chemical engineer in the Materials and Structural Systems Division, National Institute of Standards and Technology (NIST), Gaithersburg, MD. He is a member of ACI committees 231, Properties of Concrete at Early Ages; 232, Fly Ash in Concrete; 308, Curing Concrete; and 546, Repair of Concrete. His research interests include experimental and computer modeling studies of the microstructure and performance of cement-based materials.

Daniel Hussey is a Physicist at the National Institute of Standards and Technology, which he first joined as a National Research Council Postdoctoral Fellow. He received his PhD in Physics from Indiana University, Bloomington, and his BS in physics from the University of New Hampshire. His research interests are focused on neutron imaging and optics and the application of neutron imaging and scattering techniques to problems of porous media.

David Jacobson is a Physicist at the National Institute of Standards and Technology, which he first joined as a National Research Council Postdoctoral Fellow. He received his PhD in Physics from the University of Missouri, Columbia, and his BS in physics from Westminster College (Missouri). His research interests are focused on neutron interferometry, imaging and optics.

1 Jason Weiss, FACI, is the Jack and Kay Hockema Professor of Civil Engineering and the Director of the

2 Pankow Laboratory at Purdue University. He earned a BAE from Penn State University and a MS and

3 PhD from Northwestern University. His research interests include shrinkage, early age behavior,

4 cracking and moisture transport in concrete.

5

6 **ABSTRACT**

7 Shrinkage Reducing Admixtures (SRAs) are increasingly being used in concrete as a method to minimize

8 shrinkage and restrained shrinkage cracking. SRAs reduce shrinkage by decreasing the surface tension of

9 the pore solution; however, SRAs also impact the fluid viscosity, contact angle and density.

10 Consequently, the absorption and desorption processes of cementitious systems containing SRA are

11 altered. This paper describes experimental measurements of drying in cementitious mortar samples with

12 and without SRAs, focusing on three components. First, solution properties (surface tension, viscosity,

13 and contact angle) were measured at different temperatures. Second, the vapor desorption curves were

14 measured and the non-linear moisture diffusion coefficient was quantified at different relative humidities

15 (degrees of saturation). Third, neutron radiography measurements were performed to visualize and

16 quantify the effect of the presence of SRA in solution on the moisture profiles and drying front generated

17 during the early stages of the drying process. The results will be discussed in terms of theoretical

18 observations in an effort to place the modeling of moisture and shrinkage gradients in concrete on a more

19 fundamental footing.

20

24

25 **INTRODUCTION**

26 Research on Shrinkage Reducing Admixtures (SRA) in concrete began in Japan in the 1980's (Sato et al.,

27 1983, Tomita. et al., 1983, Tomita et al., 1986). In the late 1990s, research in the US began to explore

28 new formulations of SRA as well (Shah et al., 1992, Bentz et al., 2001, Weiss, 1999, Weiss et al., 1998,

29 Ai and Young, 1997), as a way to reduce shrinkage and cracking in normal and high strength concrete.

This work builds on the early research to quantify the role of SRA in moisture gradients. The SRAs are chemical surfactants that are added to concrete to reduce the surface tension of the pore fluid (by as much as 50 % (Bentz, 2006, Rajabipour et al., 2007)). This reduction in surface tension reduces drying shrinkage due to the reduced capillary pressure generated and the decrease in drying rate that results in higher degrees of saturation (Weiss et al., 1999). Review articles have been developed on the use of SRAs in concrete. These articles describe how the SRAs alter the shrinkage, cracking resistance, mechanical properties and fluid transport (Weiss and Berke, 2003, Berke et al., 1997, Shah et al., 1998, ACI Committee 231, 2010, Bentz, 2006). Many of these properties are measured and related to the properties of the pore solution.

It has been generally assumed that the ionic concentration of the pore fluid has a negligible effect on the performance of SRA (i.e., miscibility in pore fluid and surface tension reduction). However, Rajabipour et al. (2007) showed that the presence of SRA in pore solution can contribute to reducing its alkalinity and consequently delay hydration and strength development of concrete containing SRA. It has also been suggested that the lower strength in mixtures containing SRA may be due to reduced water absorption during curing caused by the reduced capillary suction (Weiss et al., 1999).

Ai and Young (Ai and Young, 1997) and Pease et al. (Pease et al., 2005) have provided measures of surface tension of water-SRA solutions. Other authors (Rajabipour et al., 2007, Eberhardt, 2011) reported results of surface tension in both water-SRA solutions and pore solution-SRA solutions at one temperature. Bentz (Bentz, 2006) reported that SRA significantly increased solution viscosity at 22 °C at a 10 % concentration by mass. Villani (Villani, 2014) performed a detailed examination of the properties (surface tension and viscosity) of SRA solutions at various temperatures.

At a molecular level, surfactants (like SRA) are amphiphilic: each surfactant molecule is composed of a hydrophilic head that is covalently bonded to a hydrophobic (i.e., non-polar) tail (Zana, 2005). The hydrophilic head is attracted by polar and hydrogen bonding solvents (such as water), and oppositely charged surfaces. The hydrophobic tail is a non-polar hydrocarbon chain and is attracted by non-polar solvents (such as oil or air), but is repelled from polar molecules such as water (Rajabipour et al., 2007). Adsorption of surfactants at interfaces causes a reduction in the interfacial energy; as such, addition of SRA produces a reduction in the surface tension of the water–air (i.e., liquid–vapor) interface.

At low concentrations, SRA molecules can be present as monomers dissolved in water. However, at higher concentrations, amphiphiles tend to aggregate and form micelles. The aggregation phenomenon is associated with a threshold surfactant concentration known as the critical micelle concentration (CMC). Below the CMC, surfactant molecules are mainly adsorbed on interfaces and as such, the surface tension

is continuously reduced with increasing surfactant concentration. Above the CMC, excess surfactant molecules form micelles in the bulk water and cannot serve to further reduce the surface tension (Rajabipour et al., 2007).

Schieβl (Schießl et al., 2000) examined drying profiles in plain concrete and concrete containing SRA using electrical resistivity. They reported similar electrical resistivity profiles at early ages (implying similar moisture content). However, the resolution of the resistivity measurement seemed not sufficient for capturing differences between the plain and the SRA system during drying at early age. Bentz et al. (2001) reported a change in the drying profile in presence of SRA: while in presence of pure water the drying front remains uniform across the depth (i.e., loss of water simultaneously at all depths during drying), when SRA are present in the system a sharp drying front forms (i.e. large moisture content change within a few millimeters in depth). Reduction in penetration depth and sorptivity rate of water in dried samples containing SRA was reported by Weiss (1999) and by Sant et al. (2010). This was theoretically predicted and related to the increase in viscosity and reduction in surface tension of the fluid (Rajabipour et al., 2007, Sant et al., 2010, Weiss, 1999), as the sorptivity coefficient scales as the square root of surface tension divided by viscosity (Hall, 1994).

Radlinska et al. (Radlinska et al., 2008, Weiss et al., 2008) and Weiss et al. (2008) showed the influence of surface tension on the size of the pores emptying during drying and shrinkage over a wide range of relative humidity (RH). Eberhardt (2011) reported a change in the desorption isotherm response of systems containing SRA that showed a lower saturation (by volume) for the same RH compared to systems without shrinkage reducing admixtures.

Neutron radiography is sensitive to hydrogen and therefore can accurately quantify in situ water movement (Hussey et al., 2012). This method provides a powerful tool in quantifying water content in porous materials such as soil and plant roots (Matsushima et al., 2009, Oswald et al., 2008, Cheng et al., 2012). Researchers have applied neutron imaging to concrete to assess properties including sorptivity and porosity. Hanžič and Ilić (Hanžič and Ilić, 2003) measured the sorptivity of concrete exposed to water and three types of fuel oil. The results from neutron radiography were compared with sorptivity obtained from a gravimetric method. De Beer et al. (De Beer et al., 2005) measured porosity and sorptivity with neutron radiography and using standard procedures in the lab. There have been previous studies investigating the drying of mortar using neutron radiography (De Beer et al., 2004, Villmann et al., 2014, Trtik et al., 2011, Lura et al., 2014), but modified solutions such as SRA have yet to be investigated.

1 **RESEARCH SIGNIFICANCE**

2 Many previous studies have been conducted on Shrinkage Reducing Admixtures to quantify their effect

3 on surface tension and ultimately shrinkage reduction. However, SRAs also impact the fluid viscosity,

4 contact angle and density, thus significantly altering transport processes in concrete. The latter aspects

5 have not been investigated yet in detail in the concrete literature.

6 This paper presents a characterization of liquid properties of SRA solution at different concentrations and

7 temperature. Changes in fluid properties are then analyzed with reference to changes expected in transport

8 properties. Specifically, the influence of viscosity, surface tension and density will be discussed as it

9 relates to desorption curves, moisture diffusion coefficient and moisture profiles generated during drying.

10 The results will be discussed in terms of theoretical observations in an effort to place the modeling of

11 moisture and shrinkage gradients in concrete on a more fundamental footing.

12

13 **EXPERIMENTAL INVESTIGATION**

14 **Materials and samples preparation**

15 One commercially available shrinkage reducing admixture has been used throughout this study (Villani,

16 2014). Several solutions were prepared by mixing SRA and deionized water in different concentrations

17 (0% - 100%) for liquid property measurements; a 5 % SRA solution by mass was used to perform

18 desorption tests and neutron radiography.

19 Desorption tests and neutron radiography were performed on plain mortar samples (not containing SRA)

20 that were previously exposed to mild drying and then saturated in the 5 % SRA solution. The mortar used

21 had a water-to-cement mass ratio (*w/c*) of 0.42 and 55 % of fine aggregate by volume. The mixing

22 procedure was in accordance with ASTM C192 (ASTM C192-12a). Mortar beams (10 cm wide by 7.5 cm

23 tall by 35.5 cm in length) were cast, demolded after 24 h and then sealed in double bags for one year.

24 For desorption testing, thin slices were cut to a thickness of 0.8 mm (with a ± 0.05 mm uncertainty in the

25 thickness measurement) using a water-cooled diamond-tipped wafer saw, then exposed to drying at

26 50 °C ± 0.5 °C for 2 d and subsequently submerged in lime water or in a 5 % SRA solution for 24 h

27 before testing. A 50 mg to 70 mg portion of the slice was used for testing.

28 For neutron radiography, 75 mm by 50 mm rectangular slices were cut to 20 mm ± 1.5 mm thick with a

29 wet saw. The specimens were then placed under vacuum and evacuated to a pressure of 930 Pa ± 670 Pa

1   (7 torr ± 5 torr). After 3 h, lime water or 5 % SRA solution was introduced to the vacuum chamber. The

2   chamber remained under vacuum for an additional hour. The pump was then turned off and the mortar

3   specimen remained submerged in the solution for 18 h. Each specimen was then removed and completely

4   wrapped in aluminum tape and stored in an airtight plastic container until being imaged (approximately

5   two weeks).

6   **Liquid properties measurement**

7   Viscosity measurements were performed using an Anton-Parr rheometer[1] (model Physica MCR 301). The

8   viscosity can be quantified from the torque applied to the fluid that generates a shear force. Calibration of

9   the device was performed using a reference standard solution (Spragg et al., 2011).

10   The surface tension of the solutions was measured using a Du Noüy Ring Tensiometer (Adamson, 1990,

11   ASTM D971-12). The method is based on determining the force that is required to detach a wire ring

12   from the surface of the solution. The tensiometer was first calibrated using de-ionized water at 23 ℃,

13   whose surface tension has been considered equal to 0.071 N/m (Pease, 2005).

14   The contact angle of the SRA solutions was measured using a Rame-Hart Advanced Automated Model

15   500 goniometer (Figure 1). The liquid was dispensed using an automatic dispenser setting a drop with a

16   volume of 11 µl for deionized water and of 9 µl for SRA solutions. A sessile type of drop was created on

17   a mortar slice 4 mm ± 0.2 mm thick and previously conditioned in a 50 % ± 1 % RH and 23.0 ℃ ± 0.5 ℃

18   chamber for 3 d. The mortar slice was cut using a water-cooled diamond-tipped wafer saw. The static

19   contact angle is captured on the sessile drop by measuring the angle formed between the solid/liquid

20   interface and the liquid/vapor interface as shown in Figure 1.

---

[1] Certain trade names and company products are mentioned in the text or identified in an illustration in order to adequately specify the experimental procedure and equipment used. In no case does such identification imply recommendation or endorsement by the National Institute of Standards and Technology, nor does it imply that the products are necessarily the best available for the purpose.
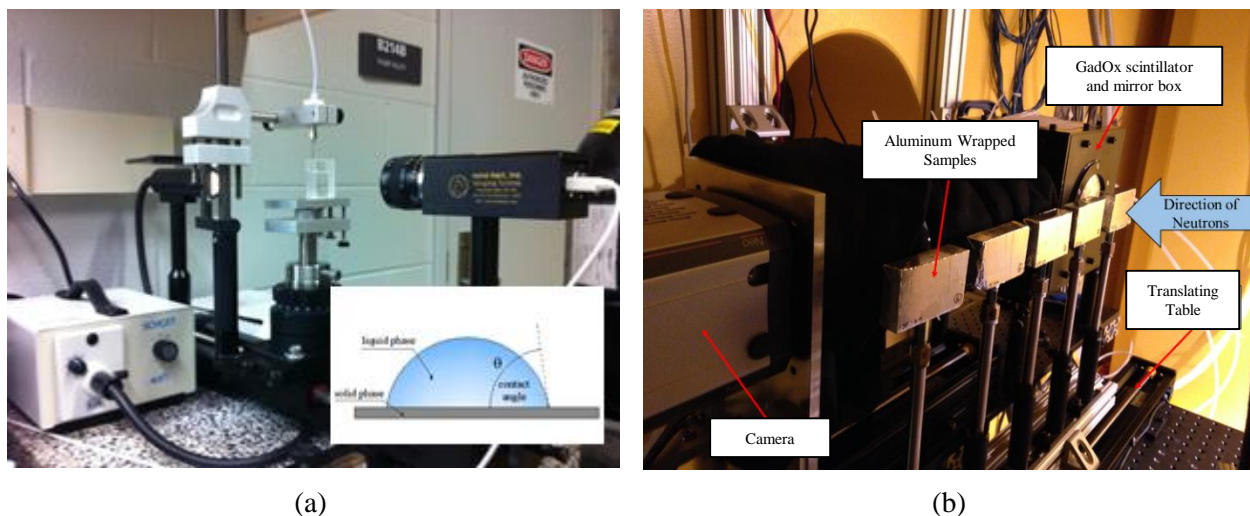
Figure 1: (a) Rame-Hart goniometer used for contact angle measurements in this study and schematic of the geometry of the pendant drop during contact angle measurement (Villani, 2014); (b) experimental set-up for neutron radiography at the Neutron Imaging Facility. The top aluminum was removed at the start of the drying experiment.

Dynamic Vapor Sorption (DVS) testing

Vapor desorption isotherms were measured using a dynamic vapor desorption analyzer (TGA Q5000), where the samples were subjected to a constant temperature while the RH was varied in controlled steps and the mass recorded as a function of time. The test started by equilibrating the sample at 97.5 % RH for either 96 h or until the sample had achieved a stable mass (less than 0.001 % mass change/15 min). The RH was then reduced in the multiple steps (96.5 %, 94.9 %, 90 %, 87.6 %, 83.8 %, 76.8 %, 70 %, 59 %, 50 % and 40 %) and the specimen finally dried to 0 % RH. The multiple steps were chosen in order to accurately capture the desorption curve at high RH where the two systems (samples containing only water and sample submerged in SRA solution) were expected to differ more substantially. The specific RH steps were chosen to empty specific size pores approximated using the Kelvin-Laplace equation, namely 40 nm, 30 nm, 20 nm, 10 nm, 8 nm, 6 nm, 4 nm, 3 nm, 2 nm and 1.5 nm, when the evaporating fluid is pure water. For each RH step, the sample was allowed to equilibrate for 12 h or 0.001 % (of initial mass of the sample) change in mass over 15 min.

Neutron Radiography

Neutron radiography was performed at the Neutron Imaging Facility at the National Institute of Standards and Technology (NIST) in Gaithersburg, MD. The beam-defining aperture had a diameter of 15 mm, a collimation ratio of 450, and a fluence rate of 1.4×10^7 $cm^{-1}s^{-1}$. A scientific complimentary oxide semiconductor (sCMOS) camera viewed a gadolinium oxysulfide scintillator through a Nikon 85 mm

1   f/1.8 lens with a PK-11a extension tube to create a neutron detector with an effective pixel pitch of

2   30 μm.

3   The experiment was set up such that five samples could be imaged in sequence. The samples were placed

4   on an automated, motorized table so that they could be positioned without the beam being turned off, as

5   shown in Figure 1. Nine reference images of the fully saturated specimens were captured, each with an

6   exposure time of 60 s. Images of similar samples cut from the same prism in the oven dried condition

7   were also taken. After taking the initial saturated images for each specimen, the top surface of the

8   specimen was exposed to the drying environment. Three images were captured before the stage moved to

9   the next position to image the next sample. As a result of the table movement, approximately 30 min

10   elapsed between each set of images per specimen. To eliminate outliers, images were combined with a

11   median filter in groups of 9 or 3 for reference or drying images, respectively. Thirty flat field (open beam)

12   and dark (closed beam) images were also taken and combined with a median filter. The use of a median

13   filter in time eliminated the appearance of streaks due to gamma rays and fast neutrons depositing energy

14   directly into the sCMOS.

15   **RESULTS**

16   **Properties of SRA solutions**

17   Experimental data for surface tension of DI water and SRA solutions measured at different temperatures

18   (10 °C, 23 °C and 38 °C) are presented in Figure 2(a). A common trend can be seen: an initial decrease of

19   surface tension for increasing SRA concentration (up to 10 % SRA concentration by mass) and

20   subsequently a constant or slightly increasing value. The change from decreasing to increasing values

21   corresponds to the saturation limit (concentration corresponding to CMC) for the number of surfactant

22   molecules that can be adsorbed on an interface; excess surfactant molecules remain in the bulk water.

23   Consequently, the reduction in the surface tension of the water−air interface is limited and reaches a

24   plateau for high surfactant concentrations (equal or higher than the CMC) (Rajabipour et al., 2007).
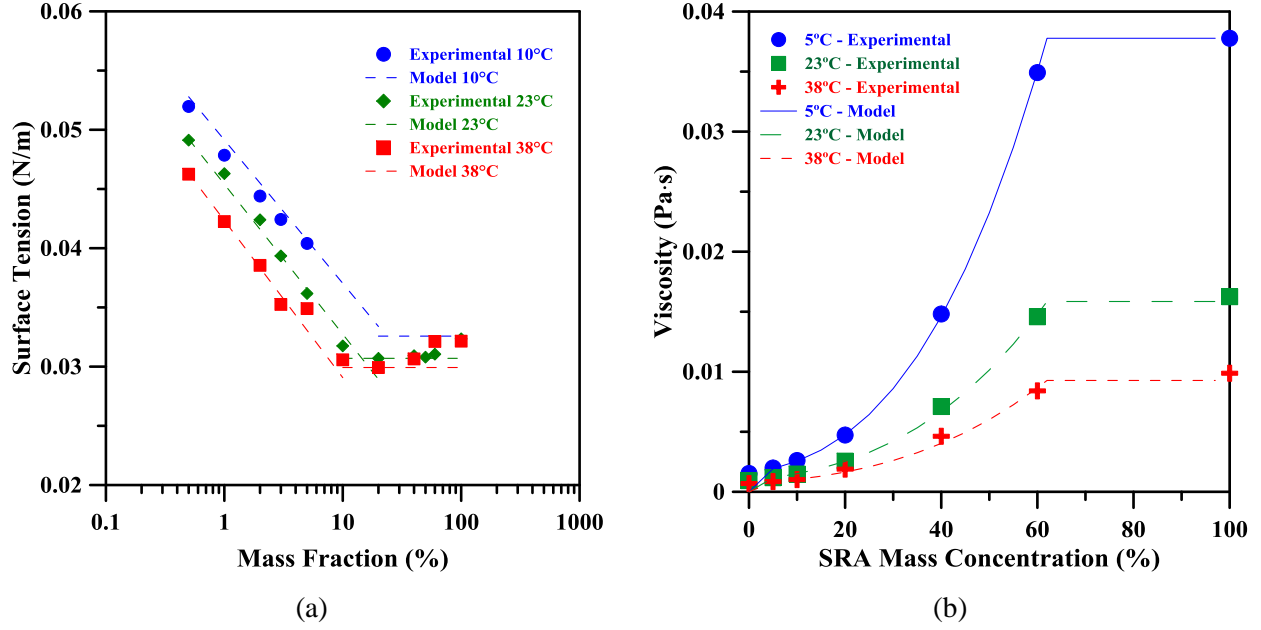
25

Figure 2: (a) Surface tension for SRA solutions in different concentrations measured with the Du Nouy Ring tensiometer (standard deviation within 0.1 % to 0.7 % for all surface tension measurements) and (b) viscosity values of SRA solutions measured with the Anton-Parr rheometer (standard deviation within 0.5 % to 1.5 % for all viscosity measurements)

1   When considering compounds that show a significant reduction in surface tension even at very low

2   aqueous concentrations, such as organic surfactants, adsorption isotherms can characterize the variation of

3   surface tension with concentration (Aumann et al., 2010, Villani, 2014). The Szyszkowski semi-empirical

4   formulation (Szyszkowski, 1908) can be used to describe the surface tension of an SRA solution at low

5   SRA concentrations (C ≤ CMC), while at higher concentrations, the surface tension is usually assumed as

6   a constant, equal to the surface tension of the pure SRA γ_{SRA} (Lura et al., 2006, Rajabipour et al., 2007).

7   The change in surface tension of SRA solution with respect to SRA concentration can then be described

8   using Equations (1) and (2):

$$\gamma = \gamma_{water} - RT\,\Gamma^{\infty}\ln\left(1 + \frac{C}{b}\right) \qquad\qquad \text{for } C < CMC(T) \tag{1}$$

$$\gamma = \gamma_{SRA} = \gamma_{water} - RT\,\Gamma^{\infty}\ln\left(1 + \frac{CMC(T)}{b}\right) \qquad \text{for } C \geq CMC(T) \tag{2}$$

9   where the surface tension γ of the solution containing C % of SRA is expressed as function of the surface

10   tension of γ_{water} (0.071 N/m at 23 °C), of the surface tension of pure SRA γ_{SRA}, of the gas constant R, of

11   the absolute temperature T and of the Langmuir adsorption coefficients Γ^{∞} and b. CMC represents the

12   critical micelle concentration for the SRA used in this study.

1 Figure 2(a) presents a comparison between experimental data and model curves (dotted lines) obtained by

2 fitting the experimental data at 23° C to Equation (1) and (2) to access the Langmuir adsorption

3 parameters ($\Gamma^\infty = 1.7310^{-6}$ mol/m^2 and b = 8.43·10^{-4} %). Equations (1) and (2) were also used to obtain the

4 predicted curves at 10 °C and 38 °C. A good correspondence between experimental data and model data

5 was obtained at all three temperatures, with the Critical Micelle Concentration a function of temperature.

6 The dependence of viscosity on mass concentration of the SRA is shown in Figure 2(b). From Figure

7 2(b), the increase in viscosity for increasing SRA concentration is evident. The non-linear increase is

8 however interrupted at concentrations approximately equal to 60 % by mass, at which point the viscosity

9 plot becomes constant. Comparing Figure 2(a) and Figure 2(b), it can be noted that the plateaus seen for

10 viscosity and surface tension do not start at the same concentration for both properties. Viscosity becomes

11 constant at some concentration above the CMC: this is likely due to the additional rheological

12 contribution seen above the CMC related to the deformation, orientation, change of the micelles (Rehage,

13 2005) or possible formation of cylindrical or lamellar structures (Bandyopadhyay and Sood, 2001).

14 Similar to the case of surface tension, the change of viscosity with respect to SRA concentration can be

15 described using a semi-empirical relation (Equation (3)) valid for $C \leq 60\%$:

$$\eta = \eta_{water} + (\eta_{SRA} - \eta_{water}) \cdot \left(C_1 V_{SRA} + C_2 V_{SRA}^2 + C_3 V_{SRA}^3\right) \tag{3}$$

16 where η_{SRA} is the viscosity of the pure SRA (0.016 Pa·s at 23 °C)), η_{water} is the viscosity of the water

17 (0.93·10^{-3} Pa·s at 23 °C), C_1, C_2, and C_3 are constants that are a function of temperature and SRA type and

18 V_{SRA} is the volume fraction of SRA. Equation (3) has been fitted to the experimental data and the

19 coefficients C_1, C_2, and C_3 have been obtained (Table 1). When the temperature increases, C_2 increases,

20 while C_1 and C_3 both decrease, causing the viscosity to increase more slowly with mass concentration.

21 The temperature dependency of viscosity for the water-SRA solutions has been also described using an

22 Arrhenius type of approach (Villani, 2014).

23

24

25

26

27

1 Table 1: Fitting coefficients from Equation (3) for water – SRA solution

T (°C)	Viscosity Water (Pa s)	Viscosity SRA (Pa s)	C_1	C_2	C_3	R^2
38	0.6784	0.0099	-0.272	-0.864	-1.820	0.99
23	0.9342	0.0163	-0.267	-0.907	-1.930	0.99
5	0.0015	0.0378	-0.167	-0.933	-2.255	0.99

2

3 The contact angle of SRA-water solutions at different concentration was also measured and the results are
4 presented in Figure 3(a). The measurements performed when pores were encountered on the exposed
5 surface were excluded in the computation of the average reported in Figure 3(a). The results shown are
6 the average among 6 to 8 measurements performed on the mortar sample surface from drops of the same
7 solution but different locations. The standard deviation resulted to be between 20 % and 35 %. To
8 confirm the trend seen, additional measurements were performed on a glass plate (with a relative standard
9 deviation between 8 % to 20 %) (Villani, 2014).

10 The contact angle appears to be influenced by the presence of SRA, especially at low SRA
11 concentrations. The addition of SRA increases the wettability of the solution up to a concentration
12 corresponding to the CMC, when the minimum contact angle is reached (Figure 3) (Chandra et al., 1996).
13 This is likely related to the reduction of surface tension. However, for higher concentrations of SRA, the
14 contact angle increases until the water contact angle is reached. It has been hypothesized that this trend is
15 related to the inversion of hydrophobic and hydrophilic groups, due to the formation of micelles (Chandra
16 et al., 1996). Changes in the capillary pressure due to the alteration of surface tension and contact angle
17 for different size pores (Young-Laplace equation (Alberty and Daniels, 1980)) were calculated and are
18 presented in Figure 3(b). Changes in surface tension contribute the most to the changes in stress
19 generated, with the contact angle having a much smaller impact.

(a)   (b)
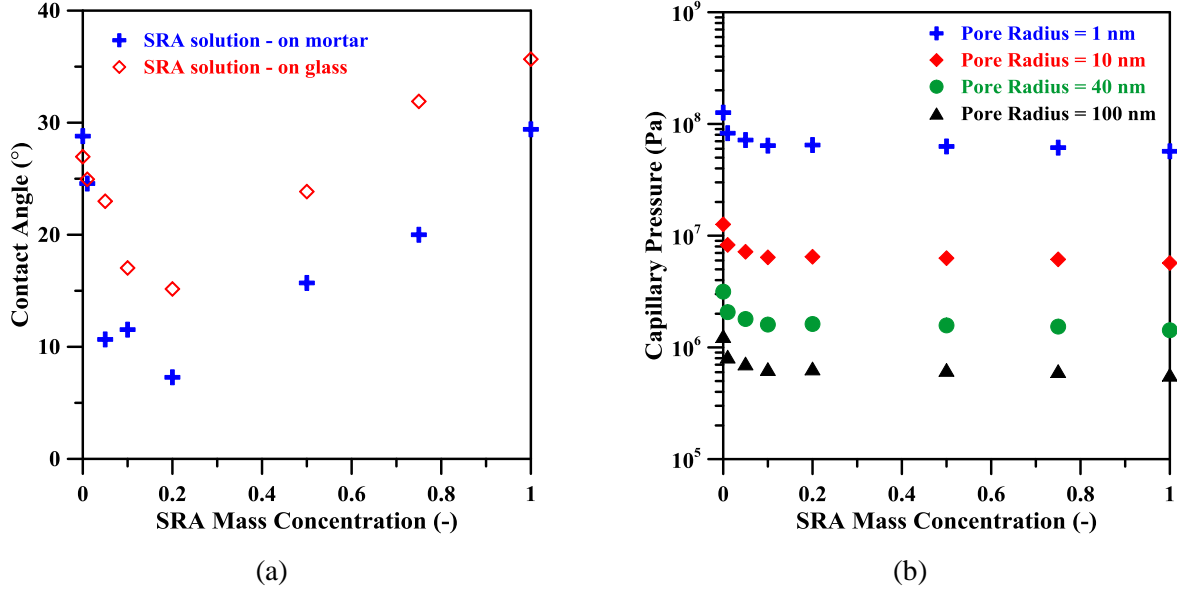
Figure 3: a) Contact angle of SRA solutions measured on mortar samples at 23 °C (standard deviation between 20 % to 35 %, (Villani, 2014)); b) Capillary pressure generated in different size pores in presence of various SRA solution concentrations

1

2   **Theoretical observations on the influence of liquid properties on drying**

3   The change in liquid properties in presence of the SRA will affect the mechanism of drying in its various

4   phases (Coussot, 2000). With reference to the three stages of drying (Constant Rate Period, First Falling

5   Rate Period and Second Falling Rate Period), the movement of fluid in the same pore structure will be

6   influenced by the changes in viscosity, surface tension and contact angle in each stage as follows. It

7   should be noted that liquid properties are continuously changing as drying occurs in a system containing

8   SRA, since water is the principal component leaving the porous system, while SRA remains, thus

9   generating a solution that becomes more and more concentrated as drying proceeds.

10   The reduction in surface tension and contact angle will increase the liquid vapor pressure, increasing the

11   evaporation speed in the C*onstant Rate Period* (Scherer, 1990), while the increase in viscosity will reduce

12   the fluid flow according to Darcy's law (Scherer, 1992). As gradients in surface tension are created in the

13   drying porous media, the Marangoni effect will cause pore solution to flow away from regions of low

14   surface tension, creating an enhanced boundary layer at the top surface in systems with SRA (Bentz,

15   2006).

16   In the two *Falling Rate Periods*, when the menisci are driven into the pores, evaporation from pendular

17   regions occurs and flow will occur. While the reductions in surface tension and contact angle tend to

18   increase the rate of evaporation in the pendular regions, the increase of viscosity of the SRA solution with

12

1   respect to pure water, along with the Marangoni effect, will decrease the flow rate of the fluid to these

2   regions.

3   Moreover, according to the Kelvin-Laplace equation at equilibrium, smaller pores will be emptied in the

4   specimens with SRA for the same external water vapor pressure (p_a), due to the reduction in surface

5   tension and of the saturated water vapor pressure (Equation (4)):

$$r = \frac{2\gamma V_m}{RT \ln(p_a/p_0)} \tag{4}$$

6   where V_m is the molar volume of the fluid and r is the capillary radius.

7   Liquid properties are also expected to influence the drying front generated. Shaw (1987) experimentally

8   proved that the width of the drying front in a porous material is inversely proportional to the square root

9   of the internal capillary pressure gradient (Shaw, 1987, Scherer, 1988) and inversely proportional to the

10 velocity of the drying front. Shaw also suggested that in the presence of fast drying, which is the case

11 studied in this work, the fluid flow is the dominant mechanism that controls the pressure gradient

12 generated across the drying front. In the presence of fluid flow, the velocity of the drying front can be

13 then related to the pressure gradient and viscosity according to Darcy's law (assuming constant

14 saturation):

$$v = -\frac{k}{\phi}\frac{\nabla P}{\mu} \tag{5}$$

15 where v is the velocity of the fluid, k is the liquid permeability, Φ is the total porosity, ∇P is the capillary

16 pressure gradient across the drying front, and μ is the viscosity of the fluid. It is hypothesized that in the

17 presence of SRA, during the first phase of drying (instantaneous) a larger pressure gradient is generated

18 as a consequence of the reduction in surface tension. The velocity of the drying front will be then

19 controlled by the combination of the effect of the increased pressure gradient and of the increased

20 viscosity.

21 **Desorption isotherms**

22 Changes in the desorption curves are also expected when liquid properties are altered. Assuming the

23 validity of the Kelvin-Laplace equation, surface tension, contact angle and density will be responsible for

24 altering the amount of fluid in equilibrium at different relative humidities. Conversely, viscosity will

25 mainly alter the rate of drying, modifying the flow of fluid in funicular conditions according to Darcy's

26 law. More specifically, the equilibrium water content at different relative humidities is supposed to

1   decrease in the presence of SRA due to the reduction in surface tension and contact angle since smaller

2   pores are emptying out (Equation (4)). Conversely, the drying time would increase due to the increase of

3   viscosity, especially when the funicular conditions are prevailing (high relative humidities).

4   The desorption curves are presented in Figure 4(a), where the equilibrium water content is shown as a

5   function of RH for the systems saturated in water and in 5 % SRA solution. It can be seen that at high

6   relative humidities, the sample containing SRA shows a lower mass at equilibrium, as expected from

7   theory. The longer drying time at high RH for the sample initially saturated in SRA solution is

8   experimentally confirmed in Figure 4(b) where it can be noticed that the equilibrium mass at 60 % RH is

9   reached after 78 h (280000 s) total testing time, while for the sample containing only water, the

10   equilibrium is reached after only 33 h (120000 s).

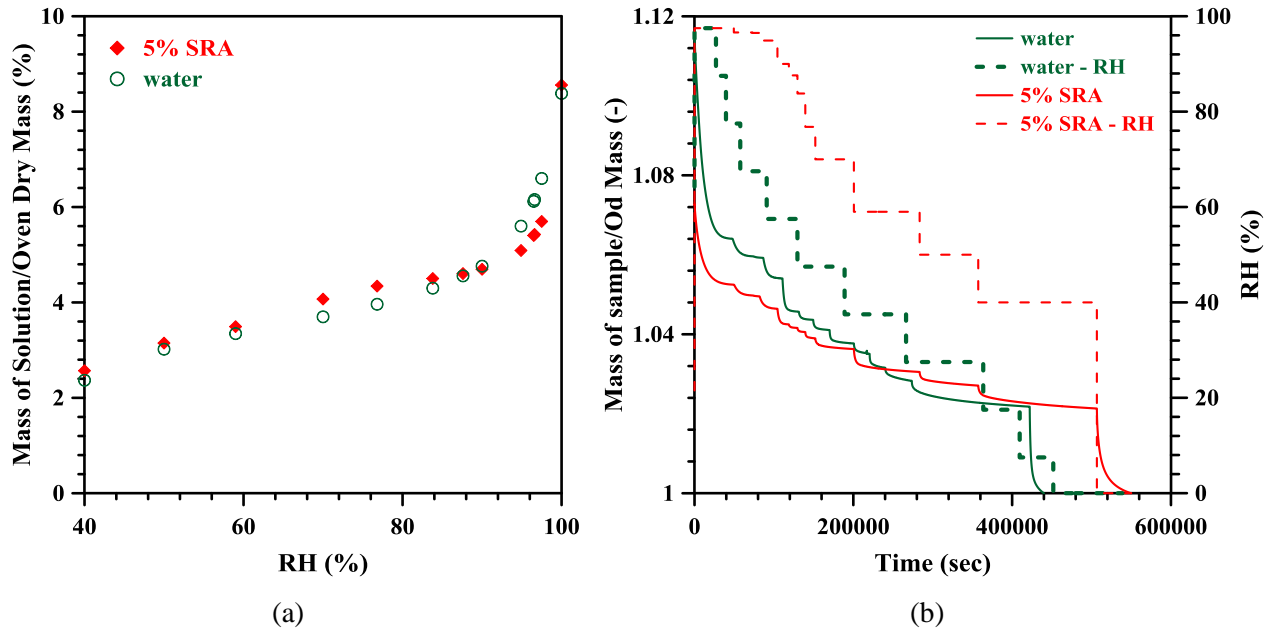(a)   (b)

Figure 4: (a) equilibrium water content for mortar saturated in water or in 5 % SRA solution (standard
deviation within 0.1 % and 0.9 % over the RH range analyzed, based on two desorption tests performed
on water saturated samples); (b) normalized mass and RH versus time during vapor desorption testing

11

12   Information on the porous structure and on the liquid properties allow one to predict changes in the

13   desorption isotherm. Changes in the desorption curve can be evaluated adopting a two-step approach:

14   First, perform a desorption test for a sample initially saturated in water to evaluate the cumulative pore

15   size distribution and vacuum saturate a sample to quantify the total porosity of the material (Bu et al.,

16   2014). The differential pore volume can then be quantified for each pore range analyzed, assuming the

17   validity of the Kelvin-Laplace equation. In this study, the last step has been done considering the density

18   of water to be equal to 1000 kg/m^3.

1   Second, assuming that no changes occur in the porous system (total porosity and pore size distribution) of

2   a fully hydrated material (degree of hydration > 85 %) during saturation in SRA solution, the desorption

3   isotherm of the system containing SRA solution can be approximately quantified considering only the

4   reduction in surface tension. The lone influence of surface tension can be considered if presenting the

5   desorption isotherm in volumetric terms and assuming the validity of the Kelvin-Laplace equation when

6   negligible changes in the liquid vapor pressure and liquid molar volume occur. For a 5 % SRA solution,

7   from Figure 2, it appears reasonable to consider the surface tension constant and equal to 0.036 N/m.

8   The comparison between the experimental desorption curve and the model is presented in Figure 5. A

9   very good correspondence between the model and the experimental curve is obtained at high relative

10   humidities, while the two curves deviate at a lower RH near 92 %, likely due to the non-uniformity of the

11   remaining (more) concentrated SRA solution.

12   However, if a gravimetric type of desorption isotherm is required, information on the density of the fluid

13   needs to be provided. Knowing the density is however challenging, since it is directly related to the mass

14   loss (i.e., the density of the solution is a function of the SRA solution concentration) which is unknown in

15   the problem. A first order approximation can be obtained assuming that water is the only component

16   leaving the system (not SRA) and that SRA does not modify the way water leaves the porous system.
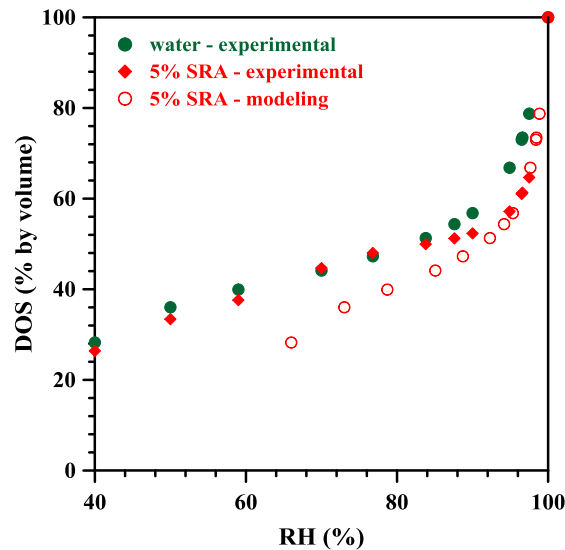

Figure 5: Experimental and modeled desorption isotherms for a cementitious mortar saturated in water and 5 % SRA solution, presented in terms of volumetric degree of saturation (DOS by volume, standard deviation between 1.1% and 9.7% for the entire RH range, based on two desorption tests performed on water saturated samples)

1 **Moisture diffusion coefficient**

2 The desorption data can further be used to quantify the non-linear diffusion coefficient with respect to RH

3 (or diffusivity with respect to water content) according to the approach proposed previously (Anderberg

4 and Wadso, 2008, Pour-Ghaz et al., 2010). This approach is valid under the assumption that the sample

5 can be approximated as a slab drying from two sides and assuming a linear change of mass over the

6 square root of time within a specific range. Figure 6 reports the diffusion coefficient with respect to RH

7 for the sample initially saturated in water and in 5 % SRA solution. The calculation has been performed in

8 this study considering the mass range corresponding to 10 % to 50 % of the total mass lost in each RH

9 step. Slower drying is confirmed for the system containing SRA that shows a lower diffusion coefficient

10 for the entire range of relative humidities compared to the sample saturated in water.

11 Changes in the diffusion coefficient when liquid properties are altered can be predicted using the

12 approach introduced by Villani et al. (Villani et al., 2014). The increase in viscosity due to SRA alters the

13 portion of the diffusion coefficient associated with liquid diffusion (i.e., high relative humidities), while

14 the surface tension alters both the vapor and the liquid portions (Villani et al., 2014, Baroghel-Bouny,

15 2007, Mainguy et al., 2001). Specifically, the increase of viscosity and the decrease of surface tension are

16 both responsible for the reduction in the diffusion coefficient as confirmed experimentally in Figure 6.
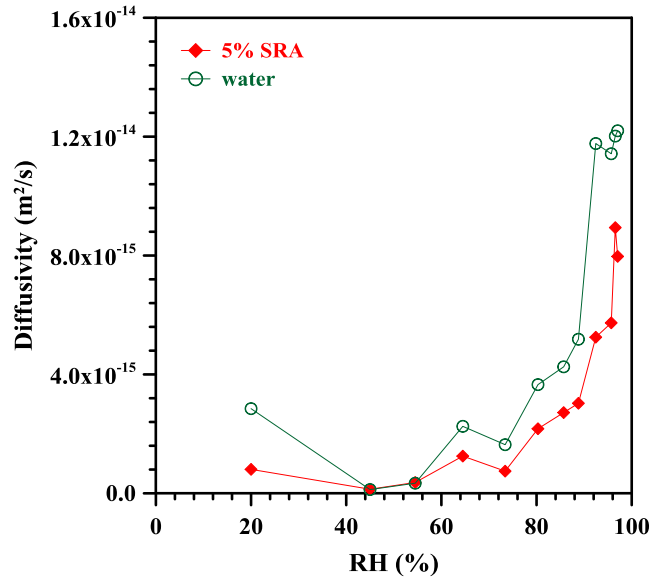

Figure 6: Diffusion coefficient with respect to RH evaluated from desorption data for samples saturated in water and 5 % SRA solution (standard deviation within $1.0 \cdot 10^{-16}$ m^2/s and $1.6 \cdot 10^{-15}$ m^2/s in the RH range considered, based on two desorption tests performed on water saturated samples)

17

18

1   **Moisture profiles**

2   The spatial change in water content was measured using neutron radiography. The water content was
3   determined for the middle third of the sample. Many researchers normalize images to an image of the
4   same sample in a completely dry state and measure the change in water content directly, if the attenuation
5   coefficient of water is known (De Beer et al., 2004, Hussey et al., 2012, Sant et al., 2010, Trtik et al.,
6   2011). Since the final goal was to determine the degree of saturation, the mass of water lost while drying
7   had to be normalized by the total volume of pores. As the volume of water that is lost from the samples is
8   smaller than an equivalent thickness of 5 mm (Lucero et al., in preparation), beam hardening effects can
9   be neglected in this analysis. Assuming the volume of pores is constant through the 20 mm cross section
10   of the mortar, the total volume of pores per pixel can be estimated by Equation 6 where the quantity
11   I_d/I_{sat} is the ratio of the average intensity of a mortar sample in the oven dried condition to the intensity
12   when completely saturated, t_{sample} is the thickness of the sample, and μ_w is the attenuation coefficient
13   of water.

$$V_{total} = \frac{\ln\left(\frac{I_{sat}}{I_d}\right)}{\mu_w t_{sample}} \tag{6}$$

14   Similarly, the change in volume of water per pixel can be computed at each position from the drying
15   edge, row i and time t. The quantity $(I_{i,t}/I_{i,0})$ is the image intensity of a sample at a specified time
16   normalized to the image intensity of that sample at time $t=0$ when fully saturated.

$$\Delta V = \frac{\ln\left(\frac{I_{i,t}}{I_{i,0}}\right)}{\mu_w t_{sample}} \tag{7}$$

17   The degree of saturation at each position from the drying edge, i and time t can be computed using
18   Equation 8. Assuming the thickness of the samples to be constant, Equation (8) has the advantage of not
19   having to measure the attenuation coefficient of water.

20

$$S_{i,t} = 1 - \frac{\ln(I_{i,0}/I_{i,t})}{\ln(I_{sat}/I_d)} \tag{8}$$

21

22   The computed degree of saturation along the sample is presented in Figure 7. The moisture gradient is
23   greater in the SRA system and initially only acts within the first 5 mm from the top drying surface. The

17

1   water system shows a highly variable gradient through the first 10 mm from the drying surface. As
2   described previously, the mortar with the SRA solution maintained a higher degree of saturation (more
3   moisture) due to a reduced diffusion coefficient. This can also be seen visually throughout the samples in
4   Figure 9. The water system appears to lose more water, particularly near the surface, compared with the
5   SRA system. Similar results, but with an even more pronounced difference in the drying fronts between
6   plain and SRA systems, have been obtained on fresh cement pastes prepared with water and with SRA
7   solutions (SRA content of 2 % by mass of cement) using X-ray transmission (Bentz et al., 2001).

(a)   (b)
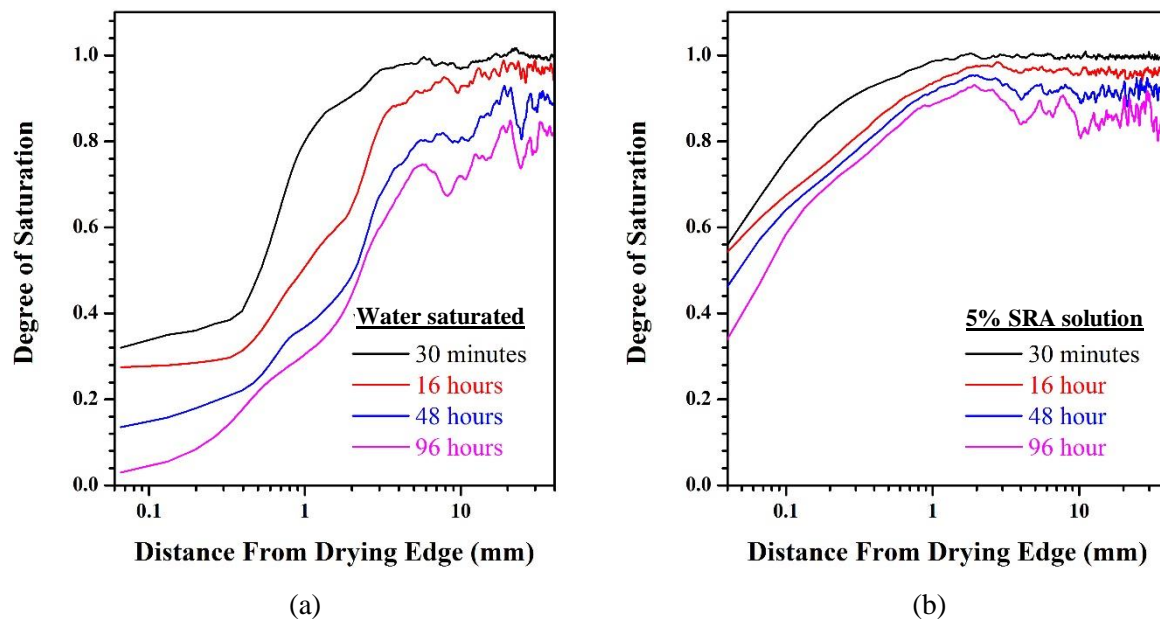
Figure 7: Average moisture profile in terms of degree of saturation for mortar samples drying from one
edge for a system saturated in (a) lime water and (b) 5% SRA solution

8

9   The results of Figure 7 can be analyzed in terms of RH or capillary pressure. In Figure 8, the degree of
10   saturation of both samples at their geometrical center after 96 h of drying has been converted into RH and
11   then into capillary pressure, using the experimental desorption isotherms and the Kelvin-Laplace
12   equation, respectively. The conversion between degree of saturation and RH has been used in the regions
13   (drying edge and geometrical center of the samples) where quasi-equilibrium conditions (i.e. stable
14   moisture content) are verified. It can be seen from Figure 7 that the capillary pressure gradient generated
15   across the drying front with respect to the edge of the sample is higher for the sample containing SRA,
16   while the width of the drying front is smaller (Shaw, 1987). The velocity of the movement of the drying
17   front (Figure 7), however, seems lower in the presence of SRA, highlighting that the effect of the
18   increased viscosity in presence of SRA is significant with respect to the effect of the capillary pressure
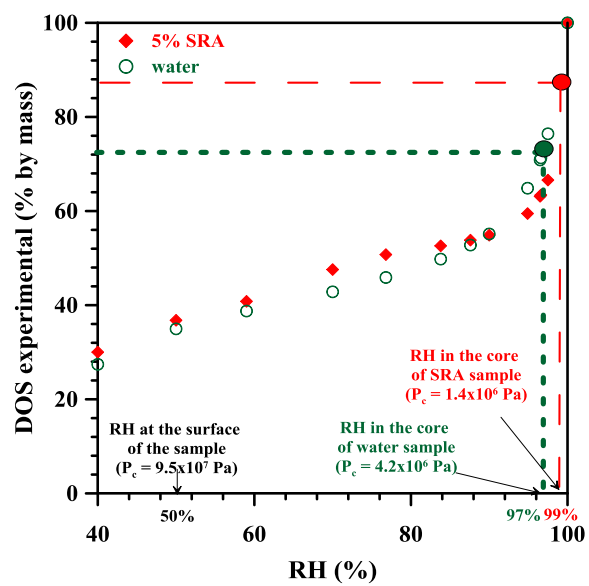19   gradient.

1

Figure 8: Relation between DOS, RH and capillary pressure in the systems containing water and SRA
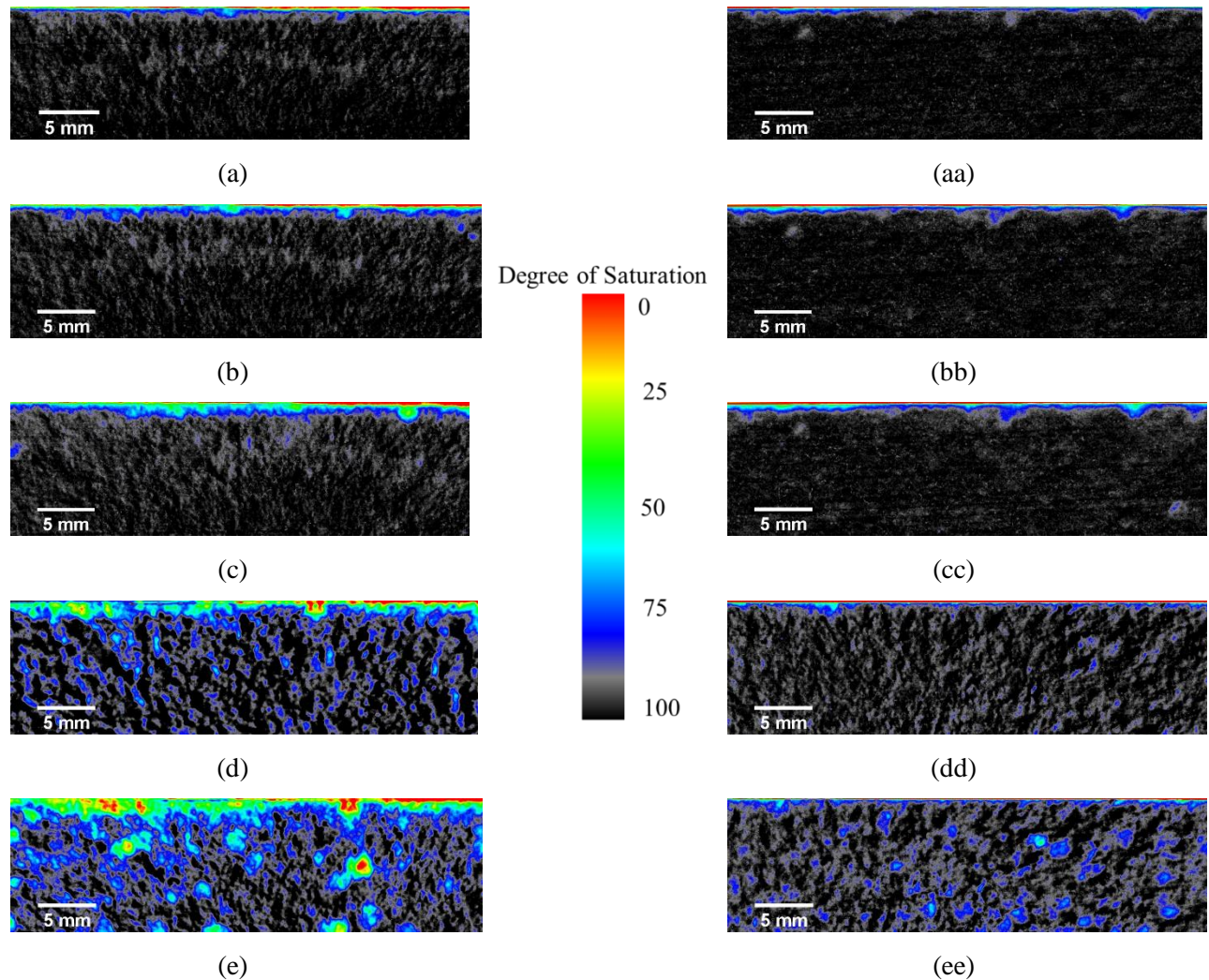
2

Figure 9: Change in the DOS in the first 12 mm from the drying surface in a mortar saturated in lime water (a,b,c,d,e) and in a mortar saturated in 5 % SRA (aa,bb,cc,dd,ee) solution at (a, aa) 30 min, (b, bb) 2.5 h, (c, cc) 6 h, (d, dd) 16 h and (e, ee) 48 h after being exposed to the drying environment.

1

2 **CONCLUSIONS**

3 Shrinkage Reducing Admixtures (SRA) have been known to reduce the capillary pressure and minimize

4 restrained shrinkage cracking by reducing surface tension of the pore solution. SRA, however, also

5 impacts other fluid properties such as viscosity, contact angle and density, resulting in alteration of

6 absorption and desorption processes in cementitious materials.

7 This work presented the characterization of SRA solution in terms of viscosity, surface tension and

8 contact angle measured at different temperatures. The changes in surface tension and viscosity were

9 considerable when SRA is present in solution, in comparison to pure water: these changes can, however,

10 be characterized using simple empirical equations.

The drying process is influenced by the presence of SRA in solution, due to the reductions of surface tension and contact angle that increase the rate of evaporation in pendular conditions. The viscosity increase of SRA solution slows the flow in funicular regions. The desorption curves will be consequently altered. Specifically, the decrease in surface tension and contact angle modified the amount of solution in equilibrium at high relative humidities ("volumetric" desorption curve) and reduced the size of pores emptying at certain RH. The increased viscosity of SRA solution extended the drying time of cementitious samples during desorption testing.

From theoretical considerations, the increase in viscosity and the reduction in surface tension would be responsible for a decrease in the moisture diffusion coefficient. This aspect was confirmed by calculating diffusion coefficient values from desorption isotherms. The diffusion coefficients were lower for the cementitious system saturated in SRA solution compared to the system saturated in water, for the entire range of relative humidities analyzed.

The effect of SRA on solution properties and further on drying was confirmed from measurements performed using neutron radiography. Moisture profiles, in terms of degree of saturation, were obtained that further confirmed the higher degree of saturation experienced in systems containing SRA related to the proven reduction of the moisture diffusion coefficient. From neutron radiography measurements, it was also possible to visualize the sharper drying front generated in the system containing SRA, which appears related to their increased internal capillary pressure gradient and higher solution viscosity.

REFERENCES

ACI COMMITTEE 231 2010. ACI 231 R-10 - Report on Early-Age Cracking: Causes, Measurement, and Mitigation. *Concrete International*. American Concrete Institute.

ADAMSON, A. W. 1990. *Physucal Chemistry of Surfaces*, John Wiley and Sons.

AI, H. & YOUNG, J. F. Mechanisms of shrinkage reduction using a chemical admixture. Proceedings of the 10th International Congress on the Chemistry of Cement, 1997. Gothenburg, Sweden, 8.

ALBERTY, R. A. & DANIELS, F. 1980. *Physical Chemistry*, New York Wiley.

ANDERBERG, A. & WADSO, L. 2008. Method for simultaneous determination of sorption isotherm and diffusivity of cement-based materials. *Cement and Concrete Research,* 38**,** 89-94.

ASTM C192-12A Standard Practice for Making and Curing Concrete Test Specimens in the Laboratory. ASTM International.

ASTM D971-12 Standard Test Method for Interfacial Tension of Oil Against Water by the Ring Method. ASTM International.

AUMANN, E., HILDEMANN, L. M. & TABAZADEH, A. 2010. Measuring and modeling the composition and temperature-dependence of surface tension for organic solutions. *Atmospheric Environment,* 44**,** 329-337.

BANDYOPADHYAY, R. & SOOD, A. 2001. Chaotic dynamics in shear-thickening surfactant solutions. *EPL (Europhysics Letters),* 56**,** 447.

BAROGHEL-BOUNY, V. 2007. Water vapour sorption experiments on hardened cementitious materials. Part II: Essential tool for assessment of transport properties and for durability prediction. *Cement and Concrete Research,* 37**,** 438-454.

BENTZ, D. P. 2006. Influence of shrinkage-reducing admixtures on early-age properties of cement pastes. *Journal of Advanced Concrete Technology,* 4**,** 423-429.

BENTZ, D. P., GEIKER, M. R. & HANSEN, K. K. 2001. Shrinkage-reducing admixtures and early-age desiccation in cement pastes and mortars. *Cement and Concrete Research,* 31**,** 1075-1085.

BERKE, N., DALLAIRE, M., HICKS, M. & KERKAR, A. 1997. New Deveopments in Shrinkage-Reducing Admixtures. *ACI Special Publication,* 173.

BU, Y., SPRAGG, R. & WEISS, J. 2014. A Discussion of the Pore Volume in Concrete as Determined Using ASTM C642 and Vacuum Saturation.

CHANDRA, S., DI MARZO, M., QIAO, Y. & TARTARINI, P. 1996. Effect of liquid-solid contact angle on droplet evaporation. *Fire safety journal,* 27**,** 141-158.

CHENG, C., KANG, M., PERFECT, E., VOISIN, S., HORITA, J., BILHEUX, H., WARREN, J., JACOBSON, D. & HUSSEY, D. 2012. Average soil water retention curves measured by neutron radiography. *Soil Science Society of America Journal,* 76**,** 1184-1191.

COUSSOT, P. 2000. Scaling approach of the convective drying of a porous medium. *The European physical journal B-condensed matter and complex systems,* 15**,** 557-566.

DE BEER, F., LE ROUX, J. & KEARSLEY, E. 2005. Testing the durability of concrete with neutron radiography. *Nuclear Instruments and Methods in Physics Research Section A: Accelerators, Spectrometers, Detectors and Associated Equipment,* 542**,** 226-231.

DE BEER, F., STRYDOM, W. & GRIESEL, E. 2004. The drying process of concrete: a neutron radiography study. *Applied radiation and isotopes,* 61**,** 617-623.

EBERHARDT, A. B. 2011. *On the mechanisms of shrinkage reducing admixtures in self con-solidating mortars and concretes.* PhD Thesis.

HALL, C. 1994. Barrier performance of concrete - A review of fluid transport theory. *Materials and Structures***,** 291-306.

HANŽIČ, L. & ILIĆ, R. 2003. Relationship between liquid sorptivity and capillarity in concrete. *Cement and Concrete Research,* 33**,** 1385-1388.

HUSSEY, D., SPERNJAK, D., WEBER, A., MUKUNDAN, R., FAIRWEATHER, J., BROSHA, E., DAVEY, J., SPENDELOW, J., JACOBSON, D. & BORUP, R. 2012. Accurate measurement of

the through-plane water content of proton-exchange membranes using neutron radiography. *Journal of Applied Physics,* 112**,** 104906.

LURA, P., MAZZOTTA, G. B., RAJABIPOUR, F., WEISS, J. & KOVLER, K. Evaporation, settlement, temperature evolution, and development of plastic shrinkage cracks in mortars with shrinkage-reducing admixtures. ConcreteLife'06-International RILEM-JCI Seminar on Concrete Durability and Service Life Planning: Curing, Crack Control, Performance in Harsh Environments, 2006. RILEM Publications SARL, 203-213.

LURA, P., WYRZYKOWSKI, M., TANG, C. & LEHMANN, E. 2014. Internal curing with lightweight aggregate produced from biomass-derived waste. *Cement and Concrete Research,* 59**,** 24-33.

MAINGUY, M., COUSSY, O. & BAROGHEL-BOUNY, V. 2001. Role of air pressure in drying of weakly permeable materials. *Journal of Engineering Mechanics***,** 582-592.

MATSUSHIMA, U., HERPPICH, W., KARDJILOV, N., GRAF, W., HILGER, A. & MANKE, I. 2009. Estimation of water flow velocity in small plants using cold neutron imaging with D< sub> 2</sub> O tracer. *Nuclear Instruments and Methods in Physics Research Section A: Accelerators, Spectrometers, Detectors and Associated Equipment,* 605**,** 146-149.

OSWALD, S. E., MENON, M., CARMINATI, A., VONTOBEL, P., LEHMANN, E. & SCHULIN, R. 2008. Quantitative imaging of infiltration, root growth, and root water uptake via neutron radiography. *Vadose Zone Journal,* 7**,** 1035-1047.

PEASE, B., SHAH, H. & WEISS, J. 2005. Shrinkage Behavior and Residual Stress Development in Mortar Containing Shrinkage Reducing Admixtures. *ACI-Special Publication on Concrete Admixtures***,** 285-302.

POUR-GHAZ, M., SPRAGG, R. & WEISS, J. Moisture profiles and diffusion coefficients in mortars containing shrinkage reducing admixtures. Proc., Int. RILEM Conf. on Use of Superabsorbent Polymers and Other New Additives in Concrete Technical, 2010. 197-206.

RADLINSKA, A., RAJABIPOUR, F., BUCHER, B., HENKENSIEFKEN, R., SANT, G. & WEISS, J. 2008. Shrinkage mitigation strategies in cementitious systems: A closer look at differences in sealed and unsealed behavior. *Transportation Research Record: Journal of the Transportation Research Board,* 2070**,** 59-67.

RAJABIPOUR, F., SANT, G. & WEISS, J. 2007. Interactions between shrinkage reducing admixtures (SRA) and cement paste's pore solution *Cement and Concrete Research,* 38**,** 606-615.

REHAGE, H. 2005. Rheological Properties of Viscoelastic Surfactant Solutions: Relationship with Micelle Dynamics. *Dynamics of Surfactants Self-Assembles.* Boca Raton, Florida: Taylor & Francis.

SANT, G., EBERHARDT, A., BENTZ, D. & WEISS, J. 2010. Influence of shrinkage-reducing admixtures on moisture absorption in cementitious materials at early ages. *Journal of Materials in Civil Engineering,* 22**,** 277-286.

SATO, T., GOTO, T. & SAKAI, K. 1983. Mechanism for reducing drying shrinkage of hardened cement by organic additives. *CAJ Review,* 5**,** 52-55.

SCHERER, G. W. 1988. Aging and drying of gels. *Journal of Non-Crystalline Solids,* 100**,** 77-92.

SCHERER, G. W. 1990. Theory of Drying. *Journal of the American Ceramic Society,* 73**,** 3-14.

SCHERER, G. W. 1992. Crack-tip stress in gels. *Journal of non-crystalline solids,* 144**,** 210-216.

SCHIEßL, A., WEISS, W., SHANE, J., BERKE, N., MASON, T. & SHAH, S. 2000. Assessing the moisture profile of drying concrete using impedance spectroscopy. *Concrete Science and Engineering(France),* 2**,** 106-116.

SHAH, S., KRGULLER, M. & SARIGAPHUTI, M. 1992. Effects of shrinkage-reducing admixtures on restrained shrinkage cracking of concrete. *ACI Materials Journal,* 89.

SHAH, S. P., WEISS, W. J. & YANG, W. 1998. Shrinkage cracking-Can it be prevented? *Concrete International,* 20.

SHAW, T. 1987. Drying as an immiscible displacement process with fluid counterflow. *Physical Review Letters,* 59**,** 1671.

SPRAGG, R., CASTRO, J., LI, W., POU-GHAZ, M., HUANG, P.-T. & WEISS, J. W. 2011. Wetting and drying of concrete using aqueous solutions containing deicing salts *Cement and Concrete Composites,* 33**,** 535-542.

SZYSZKOWSKI, B. V. 1908. Experimentelle studien über kapillare eigenschaften der wässerigen lösungen von fettsauren. *Zeitschrift für Physikalische Chemie,* 64**,** 385-414.

TOMITA, R., SIMOYAMA, Y. & INOUE, K. 1986. Properties of hardened concrete impregnated with cement shrinkage reducing agent. *CAJ Review***,** 314-317.

TOMITA., R., TAKEDA, K. & KIDOKORO, T. 1983. Drying shrinkage of concrete using cement shrinkage reducing agent. *CAJ Review***,** 198-201.

TRTIK, P., MÜNCH, B., WEISS, W., KAESTNER, A., JERJEN, I., JOSIC, L., LEHMANN, E. & LURA, P. 2011. Release of internal curing water from lightweight aggregates in cement paste investigated by neutron and X-ray tomography. *Nuclear Instruments and Methods in Physics Research Section A: Accelerators, Spectrometers, Detectors and Associated Equipment,* 651**,** 244-249.

VILLANI, C. 2014. *Transport Processes in Partially Saturated Concrete: Testing and Liquid Properties* PhD Thesis, Purdue University.

VILLANI, C., SPRAGG, R., POUR-GHAZ, M. & JASON WEISS, W. 2014. The Influence of Pore Solutions Properties on Drying in Cementitious Materials. *Journal of the American Ceramic Society,* 97**,** 386-393.

VILLMANN, B., SLOWIK, V., WITTMANN, F. H., VONTOBEL, P. & HOVIND, J. 2014. Time-dependent Moisture Distribution in Drying Cement Mortars – Results of Neutron Radiography and Inverse Analysis of Drying Tests. *Restoration of Buildings and Monuments,* 20**,** 49-62.

WEISS, J. & BERKE, N. 2003. Admixtures for reduction of shrinkage and cracking. *Report 25: Early Age Cracking in Cementitious Systems-Report*. RILEM Technical committee TC 181-EAS: Early age cracking shrinkage induced stresses and cracking in cementitious systems.

WEISS, J. W., LURA, P., RAJABIPOUR, F. & SANT, G. 2008. Performance of shrinkage-reducing admixtures at different humidities and at early ages. *ACI Materials Journal,* 105**,** 478-486.

WEISS, J. W., YANG, W. & SHAH, S. P. 1998. Shrinkage cracking of restrained concrete slabs. *Journal of Engineering Mechanics,* 124**,** 765-774.

WEISS, W., YANG, W. & SHAH, S. 1999. Factors influencing durability and early-age cracking in high strength concrete structures, High Performance Concrete: Research to Practice. *ACI Special Publication,* 186**,** 387-409.

WEISS, W. J. 1999. *Shrinkage cracking in restrained concrete slabs: Test methods, material compositions, shrinkage reducing admixtures and theoretical modeling.* PhD Thesis, Northwestern University.

ZANA, R. 2005. Introduction to surfactants and surfactants self-assemblies. *In:* FRANCIS, T. (ed.) *Dynamics of Surfactant Self-Assemblies.* Boca Raton, Florida.